Mechanisms of anisotropic friction in nanotwinned Cu revealed by atomistic simulations

2013 Modelling Simul. Mater. Sci. Eng. 21 065001

(http://iopscience.iop.org/0965-0393/21/6/065001)

Modelling Simul. Mater. Sci. Eng. **21** (2013) 065001 (16pp) doi:10.1088/0965-0393/21/6/065001

Mechanisms of anisotropic friction in nanotwinned Cu revealed by atomistic simulations

J J Zhang[1,2,4], A Hartmaier[2,4], Y J Wei[3], Y D Yan[1] and T Sun[1]

[1] Center for Precision Engineering, Harbin Institute of Technology, PO Box 413, 150001 Harbin, People's Republic of China
[2] Interdisciplinary Centre for Advanced Materials Simulation (ICAMS), Ruhr-University Bochum, 44780 Bochum, Germany
[3] State Key Laboratory of Nonlinear Mechanics, Institute of Mechanics, Chinese Academy of Sciences, Beijing 100190, People's Republic of China

E-mail: zhjj505@gmail.com and alexander.hartmaier@icams.rub.de

Received 31 January 2013, in final form 12 May 2013
Published 12 July 2013
Online at stacks.iop.org/MSMSE/21/065001

Abstract

The nature of nanocrystalline materials determines that their deformation at the grain level relies on the orientation of individual grains. In this work, we investigate the anisotropic response of nanotwinned Cu to frictional contacts during nanoscratching by means of molecular dynamics simulations. Nanotwinned Cu samples containing embedded twin boundaries parallel, inclined and perpendicular to scratching surfaces are adopted to address the effects of crystallographic orientation and inclination angle of aligned twin boundaries cutting the scratching surface. The transition in deformation mechanisms, the evolution of friction coefficients and the friction-induced microstructural changes are analyzed in detail and are related to the loading conditions and the twinned microstructures of the materials. Furthermore, the effect of twin spacing on the frictional behavior of Cu samples is studied. Our simulation results show that the crystallographic orientation strongly influences the frictional response in different ways for samples with different twin spacing, because the dominant deformation mode varies upon scratching regions of different orientations. A critical inclination angle of 26.6° gives the lowest yield strength and the highest friction coefficient, at which the plasticity is dominated by twin boundary migration and detwinning. It is demonstrated that the anisotropic frictional response of nanotwinned Cu originates from the heterogeneous localized deformation, which is strongly influenced by crystallographic orientation, twin boundary orientation and loading condition.

(Some figures may appear in colour only in the online journal)

[4] Authors to whom any correspondence should be addressed.

1. Introduction

Friction and wear, as common reasons for energy and material loss, are of both scientific and technological importance for nanostructured materials, given the minute volume of such structures [1–4]. With the emergence of advanced nanostructured materials containing hierarchic microstructures, understanding the mechanisms governing their frictional behavior on the nanoscale becomes challenging. For instance, significant effort in experimental, theoretical and computational studies on nanotwinned (NT) Cu has been made to understand the extraordinary properties of ultrafine-grained polycrystalline Cu containing embedded twin boundaries (TBs) [5–20]. Recently, some progress on the friction of NT Cu has been made experimentally and theoretically. Singh *et al* [21, 22] performed sliding contact experiments to characterize the tribological response of NT Cu. They showed that the friction evolution, the material pile up, the deformation-induced structural change and the hardness of the scratched surface strongly depend on the twin spacing and the number of repetitions of sliding cycles. On the theoretical side, Zhang *et al* [23, 24] performed atomistic simulations to show that dislocation-mediated detwinning, in addition to dislocation slip, plays an important role in the plastic deformation of NT Cu under nanoscratching. TB spacing (TBS) has a significant influence on the competition of individual deformation modes, which in turn affects NT Cu to resist scratching via plastic deformation. Despite the insights provided by previous studies, our knowledge about the role of dislocation–TB interaction played in the friction of NT Cu is still very limited. For its promising technological application in advanced functional nanostructure engineering, a fundamental understanding upon the nature of the friction of NT Cu on the atomic scale is central to the rational design of such nanostructures.

A typical friction route on NT Cu involves multiple grains, which are of different crystallographic orientations as well as the inclination angle of aligned TBs with respect to the surface. The crystallographic orientation-dependent indentation response of single-crystalline face centered cubic (fcc) metals under the localized uniaxial stress state, determined by the activation of $\{1\,1\,1\}\langle 1\,1\,0\rangle$ slip systems, has been well examined [25, 26]; however, the localized multi-axis stress state during friction causes a complex tribological response with respect to the crystallographic orientation [27, 28]. On the other side, the internal microstructures have a strong impact on the tribological response of materials [29, 30]. Compared with the dislocation activity-dominated plasticity in single-crystalline Cu, there is increased uncertainty in the crystallographic orientation dependence of the friction of NT Cu, as TBs can act as both sources and sinks for dislocations, or migrate themselves [8, 9, 12, 16, 17, 31]. Furthermore, the inclination angle is also of great importance in understanding the friction of NT Cu. While computational work on twinned metals has been extensively focusing on the twin planes perpendicular to the loading direction that leads to zero resolved shear stress within the twin planes [32–34], recent atomistic simulations and experimental investigations have demonstrated that the inclined internal twin planes with varying Schmid factors possess distinguishable dislocation–TB interactions. Stukowski and Albe [17] showed that during the tension simulation of NT Cu, dislocations glide mainly parallel to TBs in grains with a high Schmid factor, and dislocations inclined to TBs are dominant in grains with a low Schmid factor. Brown and Ghonieml [35] showed that the plasticity in twinned Cu nanopillars can be either reversible or irreversible, depending on the applied stress state controlled by the placement of TB orientation with respect to the loading axis. Furthermore, Wei [36] demonstrated that by designing the inclination angle of TBs, twin migration mediated by partial dislocation gliding in a single active slip plane can dominate the plastic deformation of one-dimensional coherent Cu nanowires. More recently, Jang *et al* [37] conducted tension experiments on

NT Cu nanopillars corroborated by atomistic simulations and reported detwinning-governed plasticity in NT nanopillars containing inclined TBs, which is different from the TB–dislocation interaction dominated plastic deformation of samples containing orthogonal TBs. Therefore, it is intriguing to explore the effect of inclination angle on the frictional response of NT Cu.

In the light of these findings reported in the literature, our focus in this work is on understanding the anisotropic friction of NT Cu, resulting from plasticity influenced by varied grain crystallographic orientation and inclination angle of aligned TBs. Without loss of physics, we consider NT Cu samples in the absence of grain boundaries (GBs) but containing twin planes that are parallel, inclined and perpendicular to the friction surface in our molecular dynamics (MD) simulations. To characterize the effects of crystallographic orientations and inclination angles, we perform nanoscratching simulations on the same surface of NT Cu samples but along different scratching directions, or along the same scratching direction but on different surfaces with varied inclination angles of the TBs cutting the surfaces. Furthermore, the effect of twin spacing on the friction of NT Cu is studied. The transition in deformation mechanisms, the evolution of friction coefficient and the friction-induced microstructure change are closely investigated. Based on such atomistic simulations, we demonstrate that the friction of NT Cu exhibits strong anisotropic characteristic, originating from the heterogeneous localized deformation caused by the competition between individual deformation mechanisms. The paper is organized as follows. In section 2, we describe details about the models of NT Cu samples, the nanoscratching procedure and the utilized defect analysis and visualization techniques. The results of friction of NT Cu with emphasis on the two aspects of crystallographic orientation and inclination angle are then presented in section 3. In section 4, we discuss the results. Finally, in section 5 we summarize the results.

2. Computational methodology

2.1. NT Cu model

In this work, we consider three sets of NT Cu samples which are characterized by how embedded TBs are arranged: aligned TBs parallel (referred to as NTP), inclined (referred to as NTI) and perpendicular (referred to as NTV) to the surface. For each set of NT Cu, we consider three twin lamellae thicknesses, such as small TBS of 0.63 nm, medium TBS of 1.25 nm and large TBS of 3.75 nm, respectively. In particular, for the NT Cu containing inclined TBs, five inclination angles, such as 0°, 26.6°, 45°, 63.4° and 90°, respectively, are considered. Figures 1(*a*)–(*c*) show the atomic configurations of these three sets of NT Cu with a TBS of 1.25 nm. The two sets of NT Cu samples containing parallel and perpendicular TBs have similar dimensions of 30 nm × 10 nm × 30 nm in X, Y and Z directions, respectively, and periodic boundary condition (PBC) is imposed in their transverse X and Z directions. For the set of NT Cu samples containing inclined TBs, however, PBC is only applied in the Z direction and the other two directions are kept free, due to the difference in lattice spacing along the X direction with respect to different inclination angles. Furthermore, to minimize the boundary effect caused by the finite size of the simulation box, the set of NT Cu samples containing inclined TBs has large dimensions of 40 nm × 10 nm × 40 nm in X, Y and Z directions, respectively. The bottom of each Cu sample is fixed to prohibit any rigid body motion during nanoscratching. The atomic interactions in Cu samples are modeled by the embedded atom method (EAM) potential developed for Cu [38]. All MD simulations are performed within the classical MD code IMD with a time step of 1 fs [39].

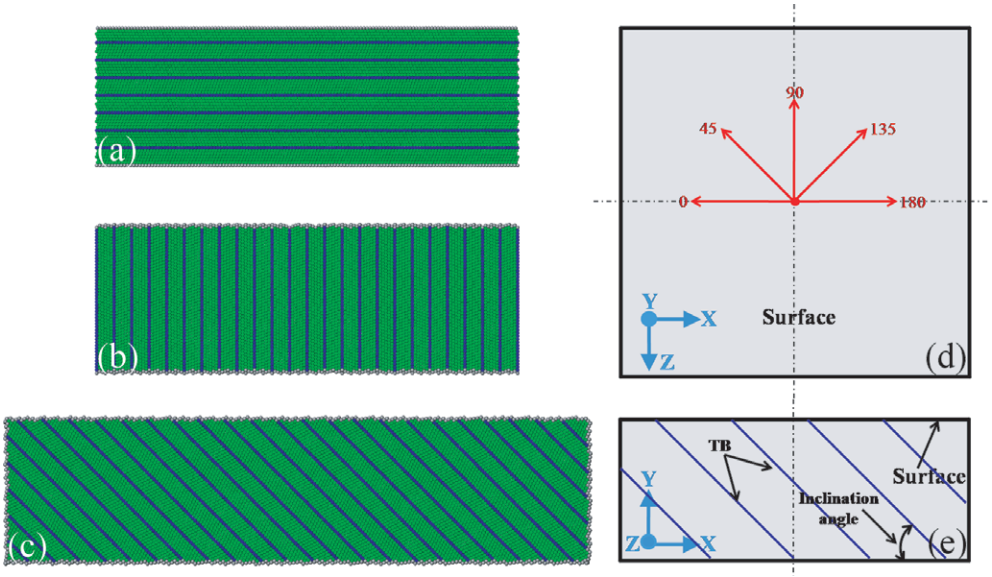

Figure 1. (*a*)–(*c*) Atomic configurations of NT Cu with a TBS of 1.25 nm. Atoms are colored according to the calculated CNA values (TBs in blue). Aligned TBs (*a*) parallel (NTP), (*b*) perpendicular (NTV) and (*c*) inclined (NTI) to the surfaces. Illustration of the strategy of studying the effect of (*d*) crystallographic orientation and (*e*) inclination angle.

2.2. Nanoscratching procedure

Prior to nanoscratching, we relax the as-created NT Cu samples to their equilibrium configurations by taking the following steps: the samples are first relaxed to their minimum energy configurations at 0 K, followed by a dynamic relaxation at 30 K and 0 bar using the Nose–Hoover thermostat for 40 ps in the isothermal–isobaric (NPT) ensemble (with constant number of particles N, constant pressure P and constant temperature T). A low temperature of 30 K is chosen to eliminate the thermal effect on underlying deformation behavior and observed frictional response of the materials. Then the equilibrated samples are subjected to nanoscratching in the microcanonical (NVE) ensemble (with constant number of particles N, constant volume V and constant internal energy E) by using a spherical frictionless probe with a radius of 8 nm. The interaction between the probe and the atoms of the material is described by a purely repulsive potential, the value of the force constant of which is 10 nN Å^{-2} [40]. The nanoscratching process involves an initial penetration and subsequent scratching. The probe first penetrates into the surface of NT Cu samples along the negative Y direction at a constant velocity of 20 m s^{-1} until it reaches the pre-determined penetration depth of 1.1 nm. Then it scratches along a fixed scratching direction at a constant velocity of 20 m s^{-1}. Both the penetration and scratching velocities of 20 m s^{-1} are seven orders of magnitude higher than typical velocities utilized in nanoscratching experiments, giving the intrinsic requirement of the integration time step to be of the order of 1 fs. To investigate the effect of crystallographic orientation for the NT Cu samples containing parallel and perpendicular TBs, we perform scratching on the same surface of each NT Cu sample but along five different scratching directions of 0°, 45°, 90°, 135° and 180°, as illustrated in figure 1(*d*). Despite the different scratching directions, the penetration of the probe remains at the same position as the center of the surface, and the scratching length is 8.1 nm. Figure 1(*e*) illustrates the investigation

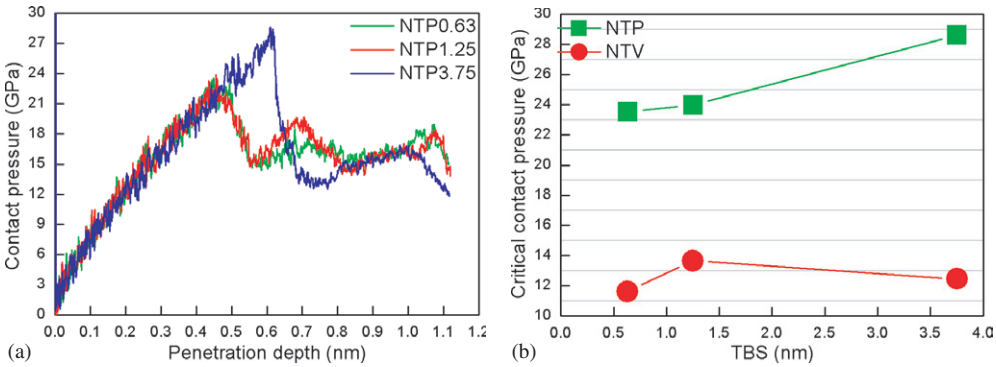

Figure 2. (*a*) Contact pressure versus penetration depth curves of penetration on the NT Cu containing parallel TBs. (*b*) Critical pressure of the NT Cu containing parallel and perpendicular TBs as a function of TBS.

of the effect of inclination angle (the angle between the scratching surface and twin planes) for the NT Cu samples containing inclined TBs, in which scratching is performed along the negative X direction with a scratching length of 14.3 nm after the completion of penetration on the right-hand side of the surface of Cu samples.

2.3. Defect analysis and visualization

The common neighbor analysis (CNA) is utilized to identify atoms of different lattice structures [41]. A single hexagonal-close-packed (hcp)-coordinated layer identifies a coherent TB, two adjacent hcp-coordinated layers indicate an intrinsic stacking fault (ISF), two hcp-coordinated layers with an fcc-coordinated layer between them represent an extrinsic stacking fault. To further distinguish TB from ISF, the novel topological analysis algorithm DXA is adopted [42]. In this work, the coloring scheme is as follows: green stands for fcc atoms, red for atoms in ISF atoms, blue for TB atoms, and gray for other atoms including free surface and dislocation cores. The Ovito is employed to visualize MD data and generate MD snapshots [43]. In addition, we also use the Atomeye to plot the morphology of the friction surface [44].

3. Results

3.1. Effect of crystallographic orientation

During the nanoscratching process, there are three force components acting on the probe, such as the scratching force along the X direction, penetration force along the Y direction and lateral force along the Z direction, respectively. The contact pressure defined as the ratio of the penetration force to the contact area is further calculated. A detailed description about the calculation of the contact area during spherical penetration can be found elsewhere [45]. Figure 2(*a*) plots the contact pressure versus penetration depth curves of penetration on the NT Cu samples containing parallel TBs. We note that the ultra-large initial contact pressures coinciding with the Y-axis in figure 2(*a*) are noises, which are produced by establishing the contact area based on limited atoms contacting with the probe at the beginning of penetration. In the initial phase of penetration the Cu sample undergoes elastic deformation, accompanied by a rapid increase in the contact pressure. After the penetration depth reaches a critical value, the contact pressure drops sharply because of a burst of initial plastic deformation

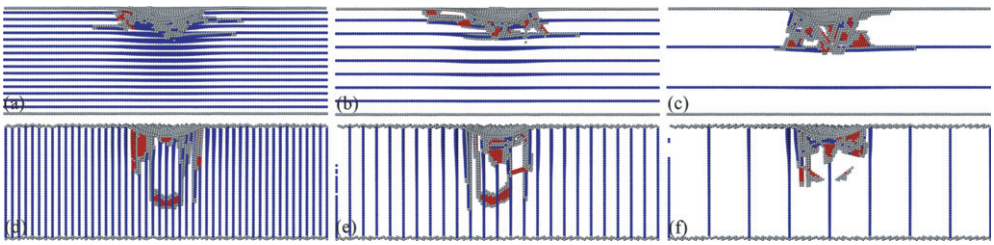

Figure 3. Cross-sectional views of instantaneous defect structures of NT Cu containing parallel and perpendicular TBs at a penetration depth of 1.1 nm. Atoms are colored according to the calculated CNA values, and fcc atoms are not shown. (*a*)–(*c*) Parallel TBs with TBS of (*a*) 0.63 nm, (*b*) 1.25 nm and (*c*) 3.75 nm; (*d*)–(*f*) perpendicular TBs with TBS of (*d*) 0.63 nm, (*e*) 1.25 nm and (*f*) 3.75 nm.

triggered by dislocation nucleation underneath the probe. The critical contact pressure is defined as the contact pressure at which the initiation of plasticity occurs. It is seen from figure 2(*a*) that although the slopes of increasing contact pressure during elastic deformation are the same for the three samples with different twin spacing, both the critical penetration depth and associated critical contact pressure for the sample with a large TBS of 3.75 nm are significantly larger than those for the other two samples with small TBS of 0.63 nm and 1.25 nm. The critical pressure of the NT Cu samples containing parallel and perpendicular TBs as a function of TBS is plotted in figure 2(*b*). For parallel TBS, the critical contact pressure for a larger TBS of 3.75 nm is higher than that for the other two small TBS. For perpendicular TBs, there is no monotonic correlation between the twin spacing and the critical pressure. Furthermore, figure 2(*b*) demonstrates that the critical pressure in the sample containing parallel TBs is approximately twice as large as that in the sample containing perpendicular TBS.

Figure 3 presents the cross-sectional views of instantaneous defect structures of the deformed NT Cu samples containing parallel and perpendicular TBs after the completion of penetration, and fcc atoms are excluded for a clearer visualization of the defect structures. It can be seen from figures 3(*a*) and (*d*) that when the twin spacing is small, lattice partial dislocations mainly glide parallel to the twin planes, and TB migration accompanied by nucleation and glide of twinning partials is another deformation mode of the Cu samples. When the twin spacing is large, however, the plastic deformation of the NT Cu samples is dominated by dislocation slip, and lattice partials inclined to the twin planes are also observed. Compared with the parallel TBs, figures 3(*d*) and (*e*) both show that there are dislocation loops cutting the perpendicular TBs formed when the twin spacing is small. Furthermore, the horizontal extension of the defect zone beneath the probe in the NT Cu containing perpendicular TBs is smaller than that in the NT Cu containing parallel ones.

The friction coefficient, defined as the ratio between scratching force and penetration force, is assessed to describe the mechanical response of NT Cu samples under scratching. Figure 4(*a*) plots the friction coefficient versus scratching length curves when scratching the NT Cu samples containing parallel TBs along the scratching direction of 0°. Despite the twin spacing, the three curves show common features: the friction coefficient increases rapidly in the initial period of scratching, and then fluctuates strongly around a constant average value when scratching is stable. The average friction coefficient is obtained by averaging more than 2000 instantaneous data points of friction coefficients within the scratching length ranging from 4.8 to 8.1 nm, as shown by the line fit for a TBS of 3.75 nm in figure 4(*a*). A longer scratching length of 11.2 nm is also studied particularly for parallel TBs with a TBS of 3.75 nm, which demonstrates that the

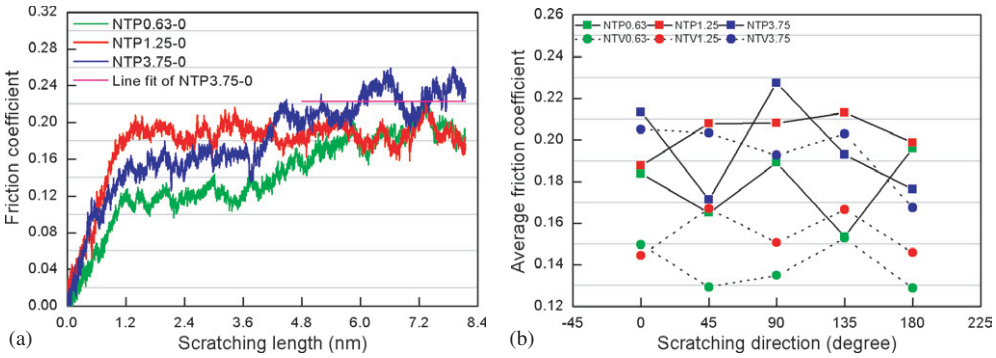

Figure 4. (*a*) Friction coefficient versus scratching length curves of scratching on the NT Cu containing parallel TBs along the scratching direction of 0°. (*b*) Average friction coefficient of the NT Cu containing parallel and perpendicular TBs as a function of the scratching direction.

convergence of the friction coefficient still holds within the longer scratching length ranging from 4.8 to 11.2 nm. Figure 4(*b*) presents the average friction coefficient of the NT Cu samples containing parallel and perpendicular TBs as a function of the scratching direction, which demonstrates that the scratching direction has a strong influence on the frictional response of the Cu samples. It is seen from figure 4(*b*) that there is no scratching direction dependence of the average friction coefficient for parallel TBs. Furthermore, the twin spacing dependence of the friction varies significantly upon the scratching direction. For instance, the friction coefficient increases with increasing TBS when the scratching direction is 0°; however, when scratching is performed along 180° the large twin spacing has a smaller value than the other two small ones. For perpendicular TBs also no scratching direction dependence of the average friction coefficient is observed. However, the average friction coefficient of the NT Cu samples containing perpendicular TBs shows strong dependence on the twin spacing: the larger the TBS, the higher the value of the average friction coefficient. We also note that the dependence of average friction on TBS may be strongly influenced by the sampling range selected, giving strong fluctuations of the friction coefficient–scratching length curves. Furthermore, under the same twin spacing the average friction coefficient for parallel TBs is higher than that for the perpendicular ones.

To reveal the deformation mechanisms governing the plastic deformation of NT Cu samples under friction, the microstructural changes are examined by analyzing defect structures generated in Cu samples. Figures 5(*a*)–(*d*) show the cross-sectional and top views of instantaneous defect structures generated in the NT Cu samples containing parallel and perpendicular TBs with TBS of 3.75 nm after scratching along 0°. It is seen from figures 5(*a*)–(*d*) that the plastic deformation of both sets of NT Cu samples is dominated by glide of lattice partial dislocations inclined to twin planes. Figure 5(*d*) shows that lattice partials cutting TBs causes the TBs to lose their coherency and trigger the nucleation of twinning partials, which leads to subsequent TB migration [9, 12, 16]. In addition, the formation of mechanical TBs shown in figure 5(*c*) indicates that deformation twinning is also an important deformation mechanism of NT Cu samples under scratching. The morphologies of the scratched surfaces of the two sets of NT Cu samples are presented in figures 5(*e*) and (*f*), respectively. It is found that the distribution of surface pile up is strongly correlated with the extent of dislocation structures beneath the surface. While surface pile up is mainly distributed in front of the probe for parallel TBs, the accumulation of materials on both sides of the scratched groove is more pronounced for the perpendicular ones.

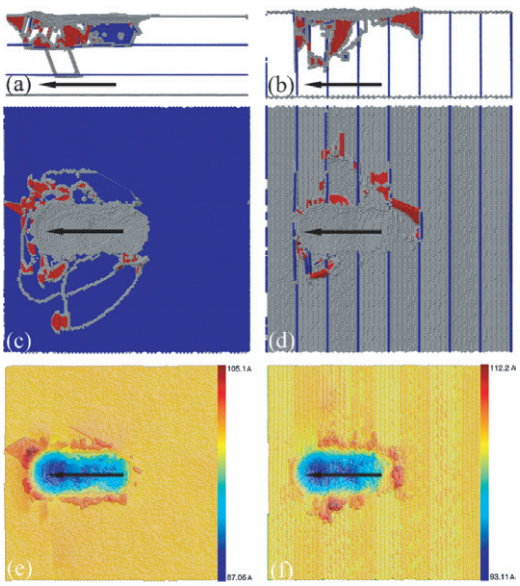

Figure 5. Structural changes of the NT Cu containing parallel and perpendicular TBs with a TBS of 3.75 nm after scratching along 0°. The scratching directions are highlighted by arrows. The top row shows the cross-sectional views of defect structures for (*a*) parallel TBs and (*b*) perpendicular TBs, and the middle row shows the top views of defect structures for (*c*) parallel TBs and (*d*) perpendicular TBs. Atoms are colored according to the calculated CNA values, and fcc atoms are not shown. The bottom row presents the morphologies of scratched surfaces for (*e*) parallel TBs and (*f*) perpendicular TBs, in which atoms are colored according to their atomic heights.

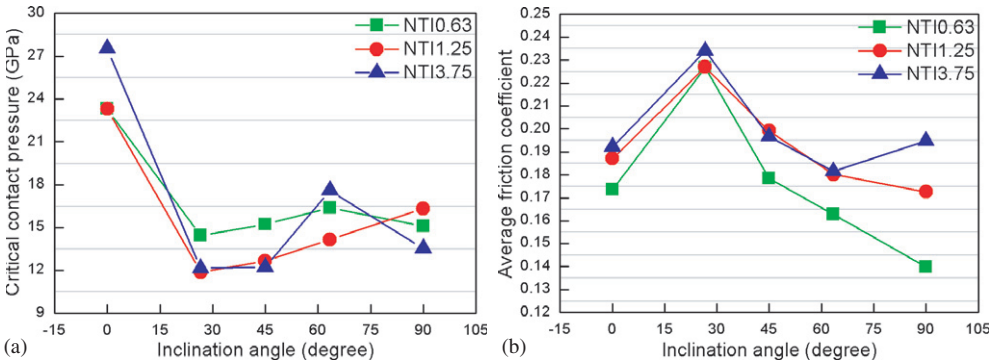

Figure 6. (*a*) Critical contact pressure of the NT Cu containing inclined TBs as a function of inclined angle. (*b*) Average friction coefficient of the NT Cu containing inclined TBs as a function of the inclined angle.

3.2. Effect of inclination angle

Figure 6(*a*) shows the critical contact pressure of the NT Cu containing inclined TBs as a function of the inclination angle, which demonstrates that the twin spacing dependence of the critical contact pressure varies significantly upon the inclination angle. It is seen from figure 6(*a*) that the NT Cu sample with an inclination angle of 0° has the highest value of critical pressure compared with the other ones, the critical pressure of which increases with

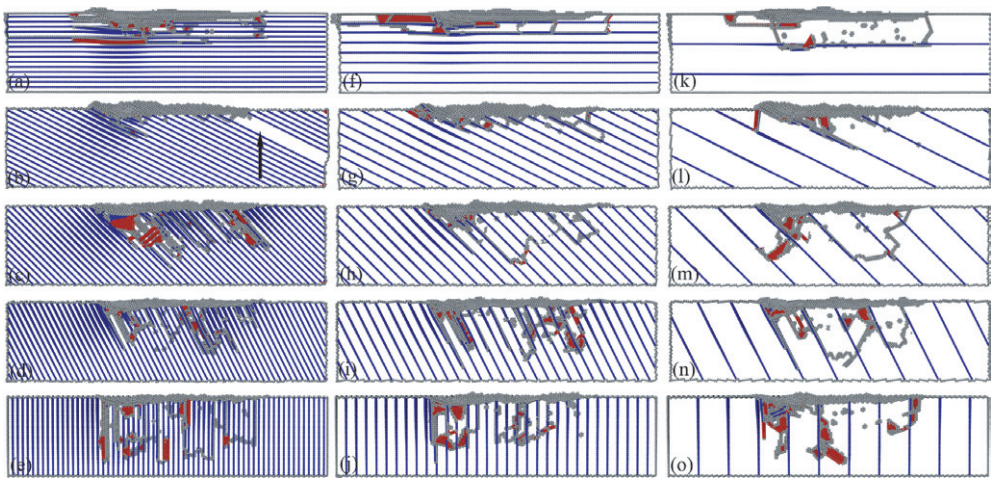

Figure 7. Cross-sectional views of instantaneous defect structures of the NT Cu containing inclined TBs after scratching. The scratching direction is the same for each sample as from right to left. Atoms are colored according to calculated CNA values, and fcc atoms are not shown. The three columns from the left- to the right-hand side are for the small, medium and large twin spacing, respectively. The five rows from top to bottom are for the inclination angles of 0°, 26.6°, 45°, 63.4° and 90°, respectively.

increasing inclination angle. Figure 6(*a*) indicates that there exists a critical inclination angle of 26.6°, at which the NT Cu sample has the minimum yield strength. Most interestingly, this critical inclination angle corresponds to the maximum value of the average friction coefficient, as shown in figure 6(*b*). The calculation of the average friction coefficient for inclined TBs is similar to parallel and perpendicular ones, but more than 3000 instantaneous data points of friction coefficients within a longer scratching length ranging from 4.8 to 14.3 nm are sampled. Furthermore, figure 6(*b*) demonstrates that the frictional resistance of the NT Cu samples containing inclined TBs strongly depends on twin spacing: the larger the TBS, the higher the value of the average friction coefficient.

Figure 7 presents cross-sectional views of instantaneous defect structures of the NT Cu containing inclined TBs after scratching, which demonstrates that the deformation behavior of the Cu samples, particularly those with a small twin spacing, is strongly affected by the inclination angle. When the TBS is 0.63 nm, figure 7(*a*) shows that lattice partial dislocations mainly glide parallel to TBs for the inclination angle of 0°, accompanied by nucleation and glide of twinning partials; however, lattice partials inclined to TBs are generally observed when the inclination angle is above the critical value of 26.6°, and detwinning becomes pronounced. Figure 7(*b*) shows that the plastic deformation of the Cu sample with the critical inclination angle is dominated by detwinning accompanied by nucleation and glide of twinning partials. The arrow in figure 7(*b*) highlights the depletion of twins, which results in the formation of a defect-free single-crystalline region. It is interesting to note that the scratching direction may have strong influence on the detwinning phenomenon shown in figure 7(*b*), as the direction of the resolved shear stress acting on twin planes changes with the scratching direction. In contrast, plastic deformation of the Cu samples with a large twin spacing, except for the critical inclination angle, is primarily controlled by dislocation activity. Figures 7(*m*) and (*n*) show that there are considerable kinks and stair-rod dislocations formed behind the probe. For the critical inclination angle with a large TBS of 3.75 nm, figure 7(*l*) demonstrates that detwinning does not occur, and TB migration resulting from partial dislocation gliding on the twin planes plays

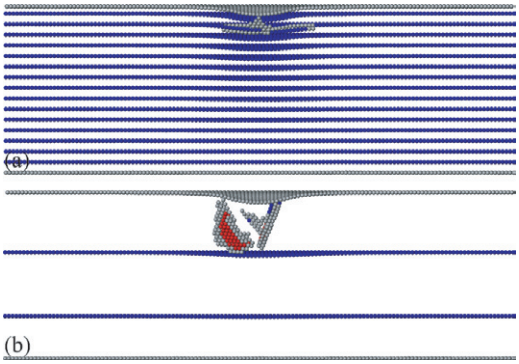

Figure 8. Cross-sectional views of instantaneous defect structures of the NT Cu containing parallel TBs with TBS of (*a*) 0.63 nm and (*b*) 3.75 nm at their critical penetration depths. Atoms are colored according to the calculated CNA values, and fcc atoms are not shown.

an important role in the plastic deformation, in addition to dislocation activity. Furthermore, both the density and extent of dislocations for the critical inclination angle are significantly lower than the other ones. It should also be noted that the influence of the perpendicular free surface in front of the probe on defect evolution is negligible; it is evidently seen from figure 7 that there is scarce dislocation activity in the vicinity of the free surface.

4. Discussion

To reveal the origin of the discrepancy between the critical contact pressures for parallel TBs shown in figure 2(*a*), dynamic evolution of the defect structures around the initiation of plasticity is analyzed. Figures 8(*a*) and (*b*) present the cross-sectional views of instantaneous defect structures of the NT Cu containing parallel TBs with TBS of 0.63 nm and 3.75 nm obtained at their critical penetration depths, respectively. It is seen from figure 8 that there is a transition of the dominant mechanism of initial plasticity accompanied by the variation of twin spacing: the initiation of plasticity for a TBS of 0.63 nm is accompanied by the nucleation of twinning partial dislocations from the pre-existing perfect TBs beneath the surface; however, initial plastic deformation for a TBS of 3.75 nm is triggered by the nucleation of lattice partial dislocations beneath the probe. Since the energy barrier to create a twin fault along a pre-existing twin plane (168.677 mJ m^{-2}) is lower than that to create an ISF (185.178 mJ m^{-2}) for Cu, the nucleation of twinning partials from perfect TBs occurs prior to the nucleation of lattice partials from the free surface under the same stress condition [46–48]. However, dislocation activity and TB-associated mechanisms work in parallel during further plastic deformation of the materials, and their strong competition leads to the convergence of the three contact pressure–penetration depth curves in the later period of penetration, as shown in figure 2(*a*).

Defect evolution plays a central role in determining the mechanical response of materials under a given applied load. Figure 9 plots the friction coefficient versus scratching length curve of scratching on the NT Cu containing parallel TBs with a TBS of 3.75 nm along the scratching direction of 0°, and two zones of dramatic friction changes are highlighted by the two red shadowed circles. To understand the origin of friction variation, an analysis of the defect evolution in the Cu sample during scratching is performed. During the initial phase of scratching, the friction coefficient exhibits a rapid increase due to the mobilization of pre-existing dislocations generated in the former penetration stage and the glide of newly

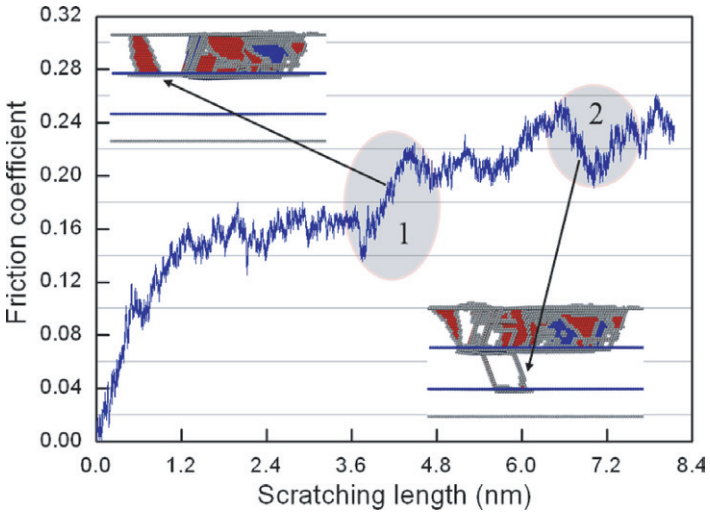

Figure 9. Friction coefficient versus scratching length curve of scratching on the NT Cu sample containing parallel TBs with a TBS of 3.75 nm along the scratching direction of 0°. The two insets present enlarged views of instantaneous defect structures at different scratching lengths. Atoms are colored according to the calculated CNA values, and fcc atoms are not shown.

nucleated dislocations. After this phase, the friction coefficient becomes approximately constant, which is accompanied by the formation of stable defect structures beneath the surface [49]. Dislocation nucleation and motion are geometrically restricted to the upper twin lamellae, where twinning partials are also nucleated due to the dislocation–TB interaction. The change in friction coefficient in zone 1 is caused by the evolution of a local defect structure beneath the probe. Upon scratching, the left upper inset of figure 9 shows that a glissile dislocation consisting of leading and trailing partials bounded by ISF separates from the defect zone in front of the probe, which leads to softening of the Cu sample accompanied by a minor decrease in the friction coefficient. Immediately after separation, however, the subsequent glide of this glissile dislocation under shear stress applied by the scratching probe increases the frictional resistance of the material, which thus results in the following rapid increase in the friction coefficient in zone 1. In contrast, the dramatic decrease in the friction coefficient in the first period of zone 2 is caused by successive nucleation of lattice partials from the first TB that gradually loses its coherency during plastic deformation. The right bottom inset of figure 9 shows the intersection of lattice partials with the second TB and formation of twinning partials. The pinning of lattice partials on the second TB increases the frictional resistance of the material; correspondingly, the friction coefficient gradually increases accompanied by a minor fluctuation in the latter phase of zone 2.

The variations of the friction coefficient for different NT Cu samples are of significant difference due to the evolution of different deformation mechanisms. A statistical analysis of the quantities of various defects is thus needed to characterize the discrepancy between different deformation mechanisms. To quantify the evolution of twin lamellae under friction with diminishing influence from pre-existing TBs, we show in figures 10(*a*) and (*b*) the changes of the normalized number of TB atoms after scratching on the NT Cu containing parallel and perpendicular TBs as a function of the scratching direction, respectively. The normalized number of TBs is assessed by dividing the evolution of TB atoms by the original number of TB atoms. The variations of the number of ISF atoms in the two sets of Cu samples are also

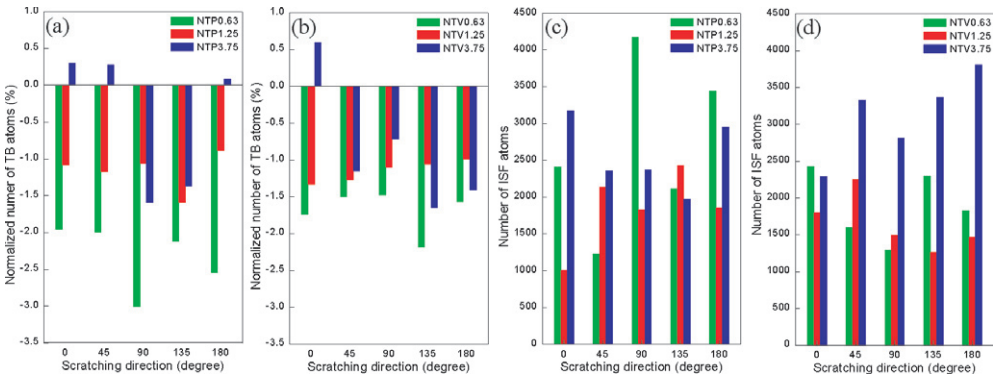

Figure 10. Evolutions in TB and ISF atoms after scratching on the NT Cu containing parallel and perpendicular TBs as a function of the scratching direction. (*a*) and (*b*) show the normalized number of TB atoms for parallel and perpendicular TBs, respectively; (*c*) and (*d*) show the number of ISF atoms for parallel and perpendicular TBs, respectively.

plotted in figures 10(*c*) and (*d*) to present the density of lattice partials. We note that the number of twinning partials is not counted due to the difficulty in distinguishing TBs that lose their coherency from perfect ones. While an increase in the number of TB atoms can be attributed to the formation of mechanical TBs through deformation twinning, its decrease is caused by detwinning. Figures 10(*a*) and (*b*) demonstrate that when the TBS is 0.63 or 1.25 nm, the number of TB atoms in both NT Cu samples containing parallel and perpendicular TBs is decreased for each scratching direction, indicating that detwinning plays an important role in the plastic deformation. For the two sets of NT Cu samples with a large TBS of 3.75 nm, however, the increased number of TB atoms after scratching along certain scratching directions is observed, which implies that deformation twinning is one mediating deformation mode in NT Cu. Recent atomistic simulation reported that deformation twinning plays an important role in the plastic deformation of nanocrystalline Cu subjected to nanoscratching [50]. It is seen from figures 10(*c*) and (*d*) that the variation of ISF atoms is not consistent with TB atoms, because the nucleation and subsequent glide of twinning partials in addition to lattice partials is also one important deformation mode of the NT Cu samples.

Figure 4(*b*) shows that for the NT Cu containing parallel TBs with a TBS of 3.75 nm, the scratching direction of 0° yields a significant higher value of the average friction coefficient than the scratching direction of 180°. To reveal the origin of this difference, figure 11 presents the cross-sectional and the top views of instantaneous defect structures of the NT Cu containing parallel TBs with a TBS of 3.75 nm after scratching along 0° and 180°. The scratching directions are highlighted by arrows. It is seen from figures 11(*a*) and (*c*) that when scratching is performed along 0°, lattice partials mainly glide inclined to TBs, and an intersection of lattice partials with the second TB is observed. In contrast, figures 11(*b*) and (*d*) show that lattice partials are primarily restricted to the first twin lamellae for the scratching direction of 180°. Furthermore, a considerable number of prismatic half-loops are formed by dislocation reactions and cross-slip events. Such glissile prismatic half-loops consisting purely of edge dislocations move parallel to the free surface and transport material displaced by the scratching probe [49]. Although the formation of mechanical TBs is observed for both scratching directions, deformation twinning is more pronounced for the scratching direction of 0° than for the scratching direction of 180°. The observations in figure 11 are inconsistent with figures 10(*a*) and (*c*), which show that the increase in the number of both TB and ISF atoms for parallel TBs with a TBS of 3.75 nm is more pronounced under the scratching direction of

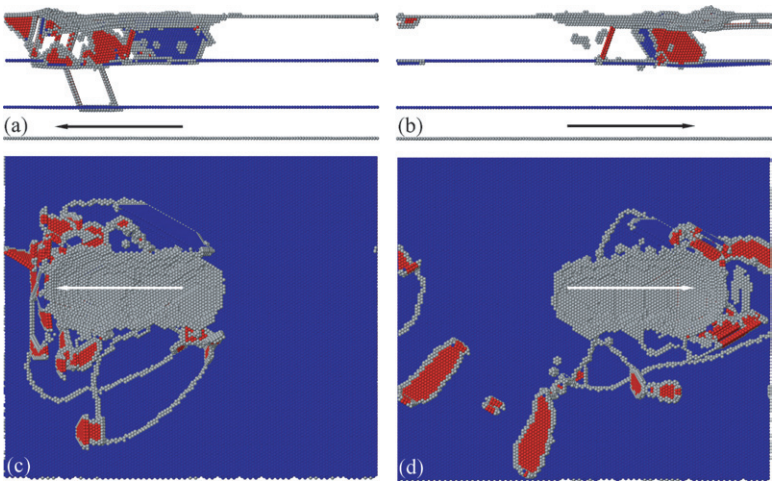

Figure 11. Defect structures of the NT Cu sample containing parallel TBs with a TBS of 3.75 nm after scratching along different directions. The scratching directions are indicated by arrows. The top row shows the cross-sectional views of scratching along (*a*) 0° and (*b*) 180°; the bottom row shows the top views of scratching along (*c*) 0° and (*d*) 180°. Atoms are colored according to the calculated CNA values, and fcc atoms are not shown.

0° than the scratching direction of 180°. Compared with inclined dislocations, the lower wear resistance associated with the easy glide of dislocations parallel to the scratching surface leads to a smaller average friction coefficient.

To reveal the origin of the critical inclination angle discovered in the NT Cu containing inclined TBs shown in figure 6, the Schmid factor for leading partial dislocation along 12 $\{1\,1\,1\}\langle 1\,1\,-\,2\rangle$ slip systems is geometrically calculated. Considering the multi-axis stress components acting on the material, the Schmid factor is divided into two components: (i) a scratching Schmid factor associated with frictional resistance along the negative X direction and (ii) a penetration Schmid factor associated with normal pressure along the negative Y direction. Table 1 lists the calculated maximum scratching and penetration Schmid factors for inclined TBs as a function of the inclination angle, which clearly indicates that the critical inclination angle of 26.6° has larger Schmid factors than the other ones. The maximum scratching Schmid factor for the critical inclination angle is 0.489, corresponding to a slip of $(1\,1\,-\,1)[1\,1\,2]$ lattice partial dislocation inclined to pre-existing twin planes. In addition to the material-dependent energy barrier reported by Jin *et al* [47, 48], the loading condition also has strong influence on the dislocation–TB interaction, in particular for NT Cu possessing comparable unstable twinning fault energy to unstable stacking fault energy. If TBs lie on high Schmid factor planes, transmission of dislocation through TBs occurs easily and blocking of dislocation motion by TBs is not significant. However, TBs residing on low Schmid factor planes act as strong obstacles to the dislocation motion as dislocations are easily nucleated on transverse glide planes [17]. Jang *et al* [37] also reported a significantly smaller tensile yield stress in the NT Cu nanopillar with inclined TBs than orthogonal ones, which originates from the distinctly different dislocation–TB interactions observed from both experiments and atomistic simulations. However, the pinning effect of transmitted dislocations increases the frictional resistance of the material, similar to the second dramatic friction change shown in figure 9. Therefore, the NT Cu containing inclined TBs with the critical inclination angle of 26.6° has the lowest yield strength and the highest frictional resistance.

Table 1. Maximum scratching and penetration Schmid factors of the NT Cu containing inclined TBs for leading partial dislocations as a function of the inclination angle.

Inclination angle	0.0°	26.6°	45.0°	63.4°	90.0°
Scratching	0.393	0.489	0.471	0.471	0.314
Penetration	0.314	0.471	0.471	0.314	0.393

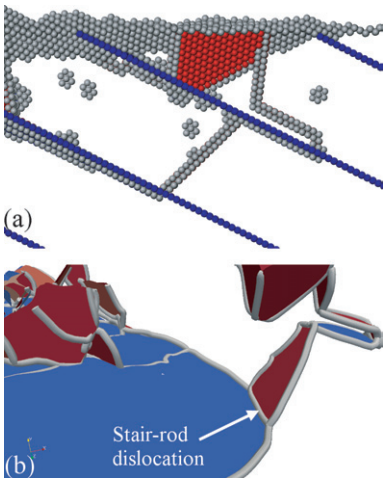

Figure 12. (*a*) Enlarged view of the local defect structure of the NT Cu containing inclined TBs with a TBS of 3.75 nm and inclination angle of 26.6° after scratching; (*b*) the dislocation network shown in (*a*).

For the NT Cu containing inclined TBs with a TBS of 3.75 nm and the critical inclination angle of 26.6°, figure 12(*a*) shows an enlarged view of the defect structures in the rear of the probe. It is seen from figure 12(*a*) that a sessile prismatic dislocation loop is formed beneath the surface, and lattice partials inclined and parallel to TBs are observed simultaneously. In particular, the lattice partials inclined to TBs exhibit mirror symmetry across the twin plane. To obtain a quantitative description of the defect structures shown in figure 12(*a*), the Burgers vector of each dislocation segment is analyzed through DXA [42] and the corresponding dislocation network is presented in figure 12(*b*). Dislocation cores are represented by gray lines, and ISF and TB are marked red and blue, respectively. It is seen from figure 12(*b*) that the dislocation cutting the second and third TBs consists of two lattice partials with $1/6\langle 1\,1\,2\rangle$ type of Burgers vector; and two twinning partials with the same $1/6\langle 1\,1\,2\rangle$ type of Burgers vector are formed on the third twin plane. Furthermore, there is a sessile stair-rod dislocation with Burgers vector of $1/6[-1\,1\,0]$ residing on the third twin plane. The formation of stair-rod dislocation, resulting from the cross-slip of partial dislocations during the incomplete transmission of the dislocation through a TB in twinned fcc metals, has also been reported elsewhere [17, 32, 54–58]. Since the Burgers vector of the formed stair-rod dislocation is perpendicular to the dislocation line but does not lie in either intersecting slip plane, it acts as an effective barrier to subsequent dislocation motion.

Previous experimental investigations and atomistic simulations have demonstrated that the plastic deformation of polycrystalline NT Cu under friction is governed by several individual deformation mechanisms working in parallel, such as dislocation slip, TB migration, detwinning, deformation twinning and GB-associated mechanism [21–24]. This work further indicates that the competition between individual deformation mechanisms strongly depends

on internal microstructures and loading conditions, i.e. the dominant deformation mode varies upon crystallographic orientation, TB orientation and scratching direction, which leads to the heterogeneous deformation behavior of NT Cu. Since the macroscopically observed mechanical response of nanocrystalline materials strongly depends on the relative participation of each grain in the deformation process [12, 51–53], an anisotropic coupling of grain orientation and twin plane orientation with respect to the scratching direction significantly intensifies the heterogeneous characteristic of localized frictional deformation of polycrystalline NT Cu, which in turn affects the fractional contribution of each deformation mechanism to the overall frictional response.

5. Summary

In summary, we performed MD simulations to investigate the deformation mechanisms, the response to friction and the microstructural changes of NT Cu samples under nanoscratching. Simulation results show that an increase in twin spacing always results in a larger effective friction coefficient if twin planes are not parallel to the scratching direction. In the case of scratching parallel to twin planes, however, the friction coefficient does not show a monotonic dependence on twin spacing. Furthermore, for the same twin spacing, scratching on parallel TBs generally results in a higher average friction coefficient than that for perpendicular or inclined TBs. It is found that the dependence of friction on twin spacing varies significantly with the scratching direction, because the dislocation–TB interaction can be strongly influenced by crystallographic orientation. The inclination angle of aligned twin boundaries cutting the scratching surface is found to be another major factor influencing the twin spacing dependence of the friction coefficient. In particular for inclined TBs, there exists a critical inclination angle of 26.6° at which the material shows the minimum yield strength and the maximum friction coefficient. Our simulations reveal that in this case the plastic deformation is dominated by TB migration and detwinning. This work demonstrates that the random coupling of crystallographic orientation and twin boundary orientation with respect to the scratching direction strongly influences the competition between individual deformation mechanisms, which in turn affects the fractional contribution of each deformation mechanism to the overall frictional response and consequently results in the observed anisotropic characteristic of the friction of NT Cu.

Acknowledgments

JZ and AH acknowledge financial support from ThyssenKrupp AG, Bayer MaterialScience AG, Salzgitter Mannesmann Forschung GmbH, Robert Bosch GmbH, Benteler Stahl/Rohr GmbH, Bayer Technology Services GmbH and the state of North-Rhine Westphalia as well as the European Commission in the framework of the European Regional Development Fund (ERDF). JZ, YY and TS also gratefully acknowledge financial support from the NSFC (51222504), the Author of National Excellent Doctoral Dissertation of PR China (201031), China Postdoctoral Science Foundation (2012M511463) and the Heilongjiang Postdoctoral Foundation of China (LBH-Z11143). YW acknowledges support from the Chinese Academy of Sciences (Hundred Talent Programme) and the NSFC (11021262).

References

[1] Bhushan B, Israelachvili J N and Landman U 1995 *Nature* **374** 607–16
[2] Tambe N S and Bhushan B 2008 *Phil. Trans. R. Soc.* A **366** 1405–24

[3] Szlufarska I, Chandross M and Carpick R W 2008 *J. Phys. D: Appl. Phys.* **41** 123001
[4] Mo Y F, Turner K T and Szlufarska I 2009 *Nature* **457** 1116–9
[5] Lu L, Shen Y F, Chen X H, Qian L H and Lu K 2004 *Science* **304** 422–6
[6] Ma E, Wang Y M, Lu Q H, Sui M L, Lu L and Lu K 2004 *Appl. Phys. Lett.* **85** 4932–4
[7] Dao M, Lu L, Shen Y F and Suresh S 2006 *Acta Mater.* **54** 5421–32
[8] Zhu T, Li J, Samanta A, Kim H G and Suresh S 2007 *Proc. Natl Acad. Sci. USA* **104** 3031–6
[9] Cao A J and Wei Y G 2007 *J. Appl. Phys.* **102** 083511
[10] Jerusalem A, Dao M, Suresh S and Radovitzky R 2008 *Acta Mater.* **56** 4647–57
[11] Anderoglu O, Misra A, Wang H, Ronning F, Hundley M F and Zhang X 2008 *Appl. Phys. Lett.* **93** 083108
[12] Shabib I and Miller R E 2009 *Acta Mater.* **57** 4364–73
[13] Li L and Ghoniem N M 2009 *Phys. Rev.* B **79** 075444
[14] Zheng Y G, Lu J, Zhang H W and Chen Z 2009 *Scr. Mater.* **60** 508–11
[15] Kulkarni Y and Asaro R J 2009 *Acta Mater.* **57** 4835–44
[16] Qu S X and Zhou H F 2010 *Nanotechnology* **21** 335704
[17] Stukowski A and Albe K 2010 *Phys. Rev.* B **82** 224103
[18] Li X Y, Wei Y J, Lu L, Lu K and Gao H J 2010 *Nature* **464** 877–80
[19] Hodge A M, Furnish T A, Shute C J, Liao Y, Huang X, Hong C S, Zhu Y T, Barbee T W and Weertman J R 2012 *Scr. Mater.* **66** 872–7
[20] Wu Z X, Zhang Y W, Jhon M H, Greer J R and Srolovitz D J 2013 *Acta Mater.* **61** 1831–42
[21] Singh A, Dao M, Lu L and Suresh S 2011 *Acta Mater.* **59** 7311–24
[22] Singh A, Tao N R, Dao M and Suresh S 2012 *Scr. Mater.* **66** 849–53
[23] Zhang J J, Sun T, Yan Y D, He Y S, Liang Y C and Dong S 2011 *J. Comput. Theor. Nanosci.* **8** 2344–9
[24] Zhang J J, Wei Y J, Sun T, Hartmaier A, Yan Y D and Li X D 2012 *Phys. Rev.* B **85** 054109
[25] Wang Y, Raabe D, Kluber C and Rsters F 2004 *Acta Mater.* **52** 2229–38
[26] Liu Y, Varghess S, Ma J, Yoshino M, Lu H and Komanduri R 2008 *Int. J. Plast.* **24** 1990–2015
[27] Grillo S E, Field J E and van Bouwelen F M 2000 *J. Phys. D: Appl. Phys.* **33** 985–90
[28] Efeoglu I and Bulbul F 2005 *Wear* **258** 852–60
[29] Renouf M, Massi F, Fillot N and Saulot A 2011 *Tribol. Int.* **44** 834–44
[30] Liu X M, Liu Z L and Wei Y G 2012 *Tribol. Lett.* **46** 167–78
[31] Wang Y B, Wu B and Sui M L 2008 *Appl. Phys. Lett.* **93** 041906
[32] Cao A J, Wei Y G and Mao S X 2007 *Appl. Phys. Lett.* **90** 151909
[33] Zhang Y F and Huang H C 2009 *Nanoscale Res. Lett.* **4** 34–8
[34] Deng C and Sansoz F 2009 *Acta Mater.* **57** 6090–101
[35] Brown J A and Ghoniem N M 2010 *Acta Mater.* **58** 886–94
[36] Wei Y J 2011 *Phys. Rev.* B **84** 014107
[37] Jang D C, Li X Y, Gao H J and Greer J R 2012 *Nature Nanotechnol.* **7** 594–601
[38] Mishin Y, Mehl M J, Papaconstantopoulos D A, Voter A F and Kress J D 2001 *Phys. Rev.* B **63** 224106
[39] Stadler J, Mikulla R and Trebin H R 1997 *Int. J. Mod. Phys.* C **8** 1131–40
[40] Kelchner C L, Plimpton S J and Hamilton J C 1998 *Phys. Rev.* B **58** 11085–8
[41] Honeycutt J D and Andersen H C 1987 *J. Phys. Chem.* **91** 4950–63
[42] Stukowski A and Albe K 2010 *Modelling Simul. Mater. Sci. Eng.* **18** 025016
[43] Stukowski A 2010 *Modelling Simul. Mater. Sci. Eng.* **18** 015012
[44] Li J 2003 *Modelling Simul. Mater. Sci. Eng.* **11** 173–7
[45] Ziegenhain G, Urbassek H M and Hartmaier A 2010 *J. Appl. Phys.* **107** 061807
[46] Sun J P, Fang L, Sun K and Han J 2011 *Scr. Mater.* **65** 501–4
[47] Jin Z H, Gumbsch P, Ma E, Albe K, Lu K, Hahn H and Gleiter H 2006 *Scr. Mater.* **54** 1163–8
[48] Jin Z H, Gumbsch P, Albe K, Ma E, Lu K, Gleiter H and Hann H 2008 *Acta Mater.* **56** 1126–35
[49] Zhang J J, Sun T, Hartmaier A and Yan Y D 2012 *Comput. Mater. Sci.* **59** 14–21
[50] Zhang J J, Sun T, Yan Y D, Dong S and Li X D 2012 *J. Appl. Phys.* **112** 073526
[51] Shabib I and Miller R E 2009 *Modelling Simul. Mater. Sci. Eng.* **17** 055009
[52] You Z S, Lu L and Lu K 2011 *Acta Mater.* **59** 6927–37
[53] Li X Y, Wei Y J, Yang W and Gao H J 2009 *Proc. Natl Acad. Sci. USA* **106** 16108–13
[54] Yamakov V, Wolf D, Phillpot S R and Gleiter H 2003 *Acta Mater.* **51** 4135–47
[55] Wu Z X, Zhang Y W and Srolovitz D J 2009 *Acta Mater.* **57** 4508–18
[56] Yang Z Q, Chisholm M F, He L L, Pennycook S J and Ye H Q 2012 *Scr. Mater.* **67** 911–4
[57] Zhu Y T, Wu X L, Liao X Z, Narayan J, Kecskes L J and Mathaudhu S N 2011 *Acta Mater.* **59** 812–21
[58] Lee J H, Holland T B, Mukherjee A K, Zhang X H and Wang H Y 2013 *Sci. Rep.* **3** 1061